AD-A149 130 CHINESE JOURNAL OF INFRARED RESEARCH (SELECTED ARTICLES)(U) FOREIGN TECHNOLOGY DIV WRIGHT-PATTERSON AFB OH L LIN ET AL. 08 FEB 83 FTD-ID(RS)T-1854-82 1/1

UNCLASSIFIED F/G 17/5 NL

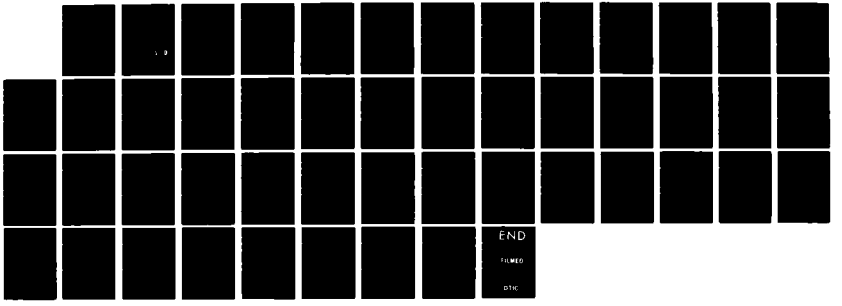

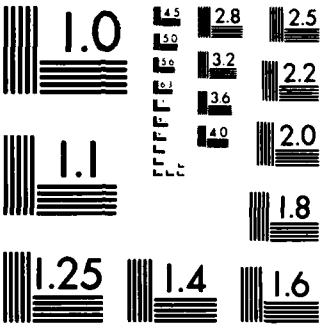

FTD-ID(RS)T-1654-82

FOREIGN TECHNOLOGY DIVISION

CHINESE JOURNAL OF INFRARED RESEARCH

(Selected Articles)

Approved for public release;
distribution unlimited.

EDITED TRANSLATION

FTD-ID(RS)T-1654-82 8 February 1983

MICROFICHE NR: FTD-83-C-000176

CHINESE JOURNAL OF INFRARED RESEARCH
(Selected Articles)

English pages: 27

Source: Hongwai Yanjiu, Vol. 1, Nr. 1, 1982, pp. 21-28; 71-76

Country of origin: China
Translated by: LEO KANNER ASSOCIATES
F33657-81-D-0264
Requester: FTD/WE

Table of Contents

GRAPHICS DISCLAIMER

All figures, graphics, tables, equations, etc. merged into this translation were extracted from the best quality copy available.

AUTOMATIC MEASUREMENT OF SPECTRAL RESPONSE OF INFARED DETECTORS

by

Lin Lin, Mu Xierun, Sun Jianbang, and Wu Binjie

Source: Chinese Journal Of Infared Research
Vol. 1 (1982) 1
Pages Translated: 21-76
Words Translated: 6,314
Translation No.: FTD-ID(RS)T-1654-82
Contractor: Leo Kanner Associates, Redwood City, CA

AUTOMATIC MEASUREMENT OF SPECTRAL RESPONSE OF INFRARED DETECTORS

Lin Lin, Mu Xierun, Sun Jianbang, and Wu Binjie
Shanghai Institute of Technical Physics, Chinese Academy of Sciences
Received 19 November 1981

The method of automatic measurement of the spectral response of infrared detectors is discussed. A special system has been built and its performances tested. The principle of the measurement and the design of the system are presented. The results show that a number of problems generally encountered in such measurements can be eliminated.

I. FOREWORD

The spectral response of infrared detectors is one of the primary characteristics of infrared detectors; the spectral response indicates the relationship between wavelength and response rate of a detector. The response-rate curve (of a detector) varying with wavelength is one of main bases of system design.

In the past, generally the measurement of relative spectral response (of an infrared detector) was conducted on a monochromator, by using point-by-point measurement. After modulation, the infrared source enters a monochromator for light dividing; the modulated monochromatic light is then

obtained. The monochromatic light is first received by a nonselective thermodetector, such as a vacuum thermocouple and heat release electric detector; a set of electric output data varying with wavelength is obtained. The data are then received by the measured detector, and similarly another set of data is obtained. By one-to-one comparison of these two sets of data, a set of spectral response data of the measured detector is then calculated. This method is relatively complex as it is time consuming. In addition, these two sets of data are not measured simultaneously; the instability of the light source and measurement equipment, as well as the environmental variation in the measurement process will bring greater error to the measurement.

For conveniently, accurately and quickly obtaining the spectral response curve of an infrared detector, the authors improved the measurement method; i.e., by using a real time comparative measurement method to divide the light (from the emission slit of the chromator) into two beams with an optical system. One light beam is received by a thermodetector, and the other light beam is received by a measured detector. Comparing signals received simultaneously by these two detectors, and processing the signals by a ratio meter, the equal-power spectral response curves of the infrared detector are directly and automatically recorded. As revealed by experimental results, the recorded equal-power spectral response curves can eliminate the effect of environmental variation and instability of the light source. Thus, the measurement accuracy and speed are increased.

II. FUNDAMENTAL PRINCIPLE OF MEASUREMENT

Under the action of the modulated monochromatic light source, the reference detector output electromotive force $V_{sth}(\lambda)$ is proportional to the spectral power distribution $\phi(\lambda)$ of the light source, the instrument function $N(\lambda)$ of the monochromator, the transparency ratio $\zeta(\lambda)$ of the monochromator, and the spectral response $G_{th}(\lambda)$ of the reference detector itself; i.e.,

$$V_{sth}(\lambda) = k\,\phi(\lambda)\,N(\lambda)\,\zeta(\lambda)\,G_{th}(\lambda), \qquad (1)$$

Under the same condition, the electromotive force $V_s(\lambda)$ (as the output of the measured detector) is similarly

$$V_s(\lambda) \propto \phi(\lambda) N(\lambda) \tau(\lambda) G(\lambda), \qquad (2)$$

In the equation, $G(\lambda)$ is the spectral response of the measured detector itself.

Comparing equations (1) and (2) and ordering them, we obtain

$$G(\lambda) = \frac{G_{th}(\lambda) V_s(\lambda)}{V_{sth}(\lambda)}. \qquad (3)$$

If $G_{th}(\lambda)$ is a constant not related to wavelength, then only by measuring $V_s(\lambda)/V_{sth}(\lambda)$ can the related spectral response of the detector be obtained. The installation we developed was made on this principle (this paper does not discuss the correction problem of $G_{th}(\lambda)$). Figure 1 shows the principle of the measurement installation.

After focusing, the infrared source is divided into two channels (upper and lower) to be separately modulated into two different frequencies. After light dividing with a monochromator, two modulated monochromatic beams (with modulated frequency) are obtained. Then the light beam with different modulated frequencies is divided into two channels to be separately received by the reference and measured detectors. After amplification and phase-sensitive detection, the energy signals simultaneously received by two detectors are divided at a ratio meter. The prism of the monochromator is rotated to synchronize with pen X of a drafting machine; then the spectral response curve (related to the measured detector) can be continuously drawn.

III. SYSTEM DESIGN

The instrument is composed of an optical system, a signal processing system, a wavelength scanning system, and a drafting machine.

1. Optical system

The optical system includes a light source, a modulator, a monochromator, and a light dividing system, as shown in Fig. 2.

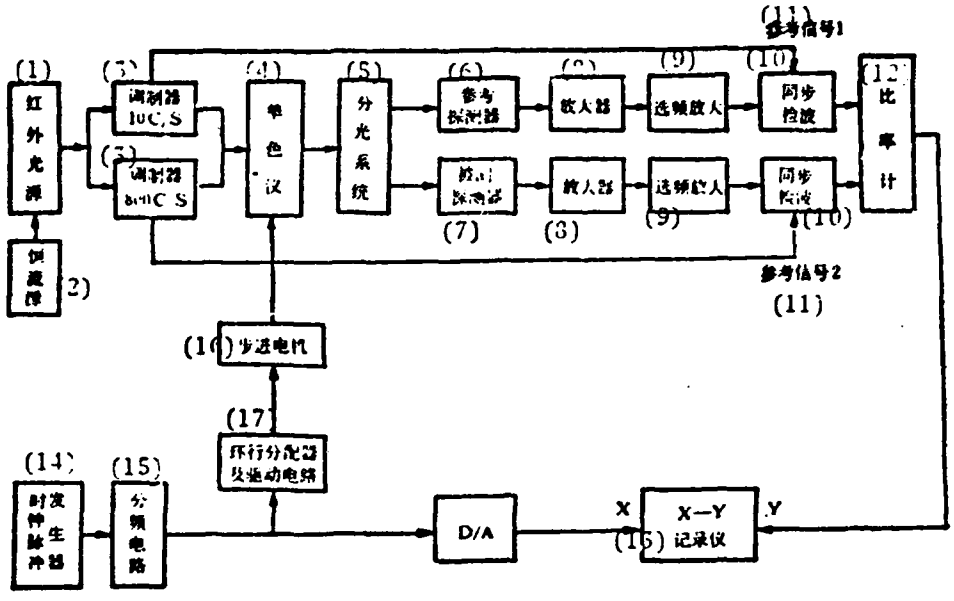

Fig. 1. Diagram showing the principle of the automatic measurement installation.
Key: (1) Infrared source; (2) Source of constant current; (3) Modulator; (4) Monochromator; (5) Light dividing system; (6) Reference detector; (7) Measured detector; (8) Amplifier; (9) Amplification of selective frequency; (10) Synchronous detection; (11) Reference signal; (12) Ratio meter; (13) Recording instrument; (14) Clock pulse producer; (15) Frequency division circuit; (16) Synchronous motor; (17) Rotary distributor and drive circuit.

The authors used a Nengsite [transliteration] lamp as the infrared source, which produces radiation in a wider wave band. The operating current of the light source is supplied by a steady current source; the operating current of the light source is continuously adjustable, generally at 0.6A.

After focusing (by a reflective mirror) of the Nengsite light source, the light beam falls on an incident slit of the monochromator with a long slender shape. A mechanical modulation device is placed between the light source and incident slit (of the monochromator). Modulations are conducted by taking one half of the upper and lower portions of the light beam. At both sides of each modulating disk, a small bulb and a silicon

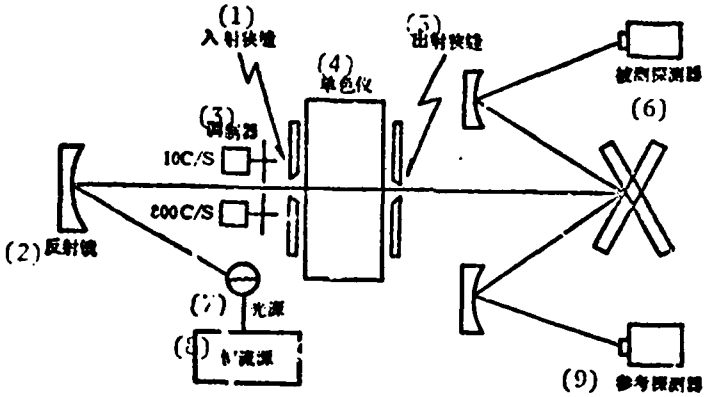

Fig. 2. Diagram showing principle of optical system. Key: (1) Incident slit; (2) Reflective mirror; (3) Modulator; (4) Monochromator; (5) Emergent slit; (6) Measured detector; (7) Light source; (8) Source of constant current; (9) Reference detector.

photoelectric diode are installed. While rotating the modulating disk, the light of the small bulb is simultaneously modulated, so that the silicon photodiode can receive the synchronizing signal of the modulating disk; the synchronizing signal is used as the reference signal of phase sensitive detection in order to obtain a greater signal-to-noise ratio. The modulation frequency is determined by the detector; if a TGS heat-release electric device is used as a reference detector, and a photoelectric type detector is used as a measured detector, then based on the characteristics of these two categories of devices, the modulation frequencies are respectively, 10 C/S and 800 C/S.

A Carl Zeiss SPM-2 type monochromator is used as the monochromator. Based on the requirements of spectral response of the measured detector, a corresponding prism is used for light division; wavelength scanning is driven by a stepped motor.

The monochromatic light modulated from the upper and lower beams (10 C/S and 800 C/S) comes from the emergent slit of the monochromator; these two beams fall separately on two (upper and lower) plain mirrors, intersecting each other at 45°. These two plain mirrors reflect the beams, separately, onto two concave mirrors, focusing on response elements of the reference and measured detectors. Thus, the two detectors simultaneously receive signals from the same light source. If the reflective characteristics of the reflective mirrors of two light channels are basically consistent, the chromatic characteristics of the light beams in both light channels are consistent; the energy ratio is constant in the measured spectral range. All optical elements and detectors are installed on a microadjustable frame with three adjustable axes in order to accurately adjust the position during measurement.

2. Signal processing system

The signal processing system includes two ports: the signal receiving circuit and the ratio meter.

The reference detector and measured detector use two corresponding (but different) prime amplifiers for detection and measurement of weak signals to separately conduct amplification and frequency selection via two channels of the main amplifier and R-C frequency selection amplifier. The center frequency of the frequency selection amplifier is consistent with the corresponding modulation frequency; the amplifier has a wider activity range and a constant increment of the energy signal received from the entire optical spectral band. In order to raise the capability of detecting and measuring signals by a circuit, the principle of the phase discriminator is adopted to separately conduct phase sensitive detection on signals. The alternating-current (ac) signals received by the detector are converted into direct-current (dc) signals to conduct signal processing by a ratio meter. The reference signals of phase sensitive detection are output from the silicon photodiode on a modulating disk. In order to adjust the phase relationship between reference signals and reception signals, an adjustable circuit has been designed in the circuit to separately conduct phase

adjustment on two channels of reference signals. The time constant of the entire circuit is primarily determined by integration time ζ of phase sensitive detection. In order to obtain a relatively good effect in phase sensitive detection, 2.5 seconds is selected as the integration time; the time constants of two channels are equal to each other.

The ratio meter is the key part of this instrument. In order to simplify the circuit configuration, a division simulator is used to meet ratio requirements. The division simulator applies the principle of the logarithmic circuit, the mathematical expression (of the simulator) is as follows:

$$V_o = \text{Antilog}\ (\log x - \log y) = x/y_o \qquad (4)$$

In the circuit of the division simulator, four computing amplifiers constitute the logarithmic and antilogarithmic circuits. Only under the condition of compatibility of four feedback transistors are computing accuracy and temperature stability quite satisfactory. Within the output range, the computing accuracy is within 2 percent.

Two channels of signals from phase sensitive detection are simultaneously sent to the input terminal of the ratio meter; the signal of the measured detector is used as numerator, and the signal of reference detector is used as denominator. When the numerator or denominator varies, the ratio meter can accurately measure the instantaneous value of the ratio. Placing the ratio signal (output from the ratio meter) onto pen Y of the recording instrument, curves can be recorded relative to spectral response When the light source or other factors induce simultaneously proportional variation in the numerator and denominator, the output of the ratio meter does not vary. This may eliminate errors caused by variation of the light source, or variations of environmental temperature and air components.

3. Wavelength scanning system

The wavelength scanning system includes a motor, a drive circuit, a D/A conversion circuit, and relay coupling circuit (for position restraint of recording pen).

The wavelength scanning of the monochromator is driven by a stepped motor. The authors directly connect the stepped motor with the wavelength adjustment hand wheel of the monochromator. Step distance of the motor is 1.5°; as the center wavelength of the monochromator varies from 0.6 μm to approximately 15 μm, the motor requires to rotate approximately 3600 steps. For a NaCl prism, smaller color dispersion is between 2μm~3 μm. For each 0.1 μm, the stepped motor should be rotated 8~9 steps. Therefore, the step distance of the stepped motor can meet the requirement of 0.1 μm accuracy in wavelength.

The motor rotating speed is considered in the following way: if the time constant of the signal processing circuit is τ, when the motor rotating speed is sufficiently low, it can ensure sufficient time (several-fold of the circuit time constant) to record the ratio-meter output corresponding to every wavelength. In order to effectively raise the testing speed, the authors first determined that 3τ, was the required testing time for each wavelength. If a point is measured at every 0.1 μm, then in the minimum linear dispersion zone, when the wavelength scanning is 0.1 μm, the time required for rotating N steps of the stepped motor is 3τ, the frequency of the stepped motor is $N/3\tau$.

According to different requirements on accuracy of the tested wavelength by different detectors, different recording speeds can be selected. At present, the motor clock frequencies the authors selected are 1 Hz, 2 Hz and 4 Hz. Supplied by clock pulse after frequency division, the recording times of 0.6 μm~15 μm are, respectively, 15 minutes, 30 minutes and 60 minutes. For 2 μm~14 μm, the recording times are, respectively, 11 minutes, 21 minutes and 42 minutes.

In order to have a simple and reliable system and to avoid errors due to instability of clock frequency, a single clock is adopted as the datum to synchronize the prism rotation and pen (X) motion of the recording instrument. After frequency division, the clock pulses are divided into two

channels. One channel passes through a circular distributor and a power amplification circuit to rotate the stepped motor. Another channel is input to a data mode switching circuit to convert clock pulses into dc signals on pen X of the recording instrument. The switching circuit is a stepped integration circuit of high-order number and long time; the integration time is as long as scores of minutes, and the number of steps is more than 3600 with each step less than 1 mV. Hence, a dc voltage (varying with time and rising proportionally) is applied on the pen X with a degree of linearity greater than 1 percent.

Since the prism color dispersion is nonlinear, the spectral scale of the recording paper should be calibrated corresponding to the scale of prism color dispersion. Thus, the spectral error recorded is less than 0.1 μm. If no voltage is applied on pen X, a method of manual dot-marking can be used (while moving the recording paper) to calibrate wavelength coordinates.

IV. MEASUREMENT RESULTS

Quite a few measurements were conducted on several different types of photoelectric detectors. As revealed by measurement results, the system can effectively test and measure the spectral response of detectors.

1. Measurements are conducted by changing the operating current (adjusted separately at 0.6 A and 0.9 A) of the light source. The relative spectral response of the measured detector is basically consistent (see Fig. 3). At different times, the authors plotted two spectroradiometric curves (of the Nengsite lamp); these two curves do not coincide (see Fig. 4). However, by conducting two corresponding tests on a single detector, the response curves are comparatively close (see Fig. 5). This explains that the system has an effective influence in eliminating light-source variation during the measurement process.

2. Comparing curves plotted by automatic measurement with the spectral response curves plotted by calculation of point-by-point measurement, using the same detector, the peak-value wavelength and the cutoff wavelength

generally coincide; the curve shapes are generally similar (see Fig. 6(a) and (b)). However, the measurement speed is more than 10 times faster.

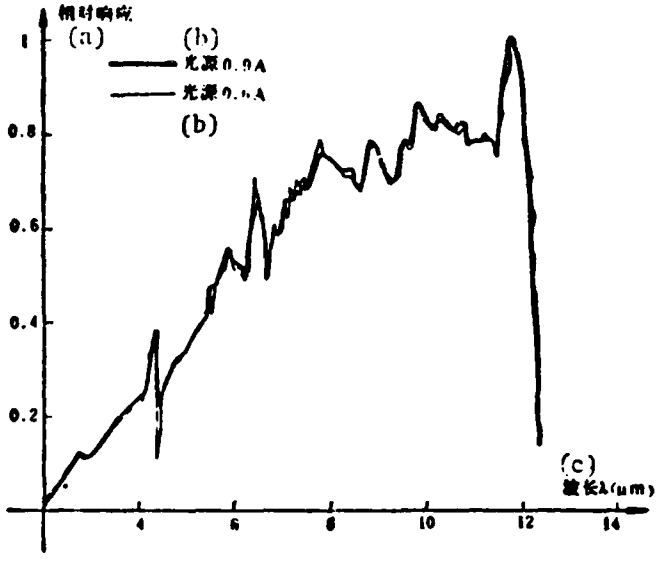

Fig. 3. Spectral response curves of HgCdTe detector for light source at different operating currents. Key: (a) Relative response; (b) Light source; (c) Wavelength.

3. Several different wave bands are selected according to performance characteristics of the measured and reference detectors; the slit width of the monochromator is changed within a certain range; and the output data of the ratio meter are generally consistent. This indicates unchanged results; although energy varies while varying slit width, by comparing two channels of real-time signals, the results remain unchanged if the numerator and denominator vary in the same proportion, as indicated in Table 1.

V. ANALYSIS OF MEASUREMENT ERRORS

1. Environmental effect

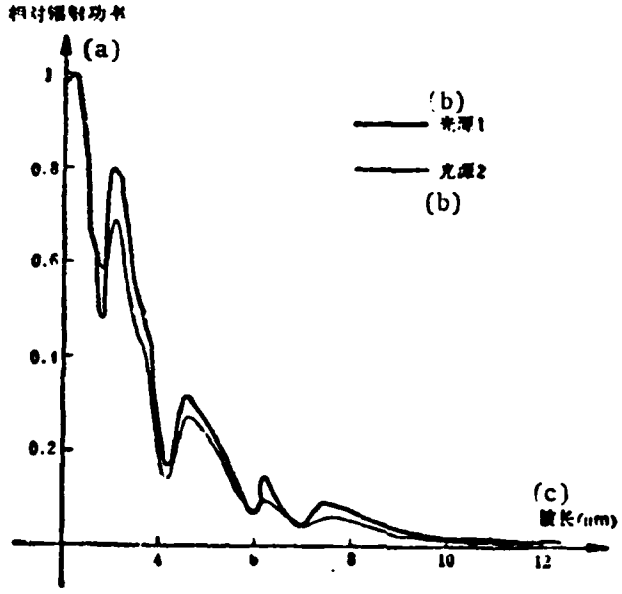

Fig. 4. Radiation curves of two different light sources.
Key: (a) Relative radiation power; (b) Light source;
(c) Wavelength.

Table 1. Radio meter outputs while varying slit width.

(a) \ (b) \ (c)	0.5mm	0.4mm	0.3mm	0.2mm
5μm	0.67 V	0.67 V	0.67 V	0.67 V
10μm	1.5 V	1.5 V	1.5 V	1.5 V

Key: (a) Wavelength; (b) Output; (c) Slit width.

Since the response wave band of the measured detector generally lies between 2 μm and 15 μm, variations of environmental temperature and atmospheric composition will introduce errors in measurement. The variation

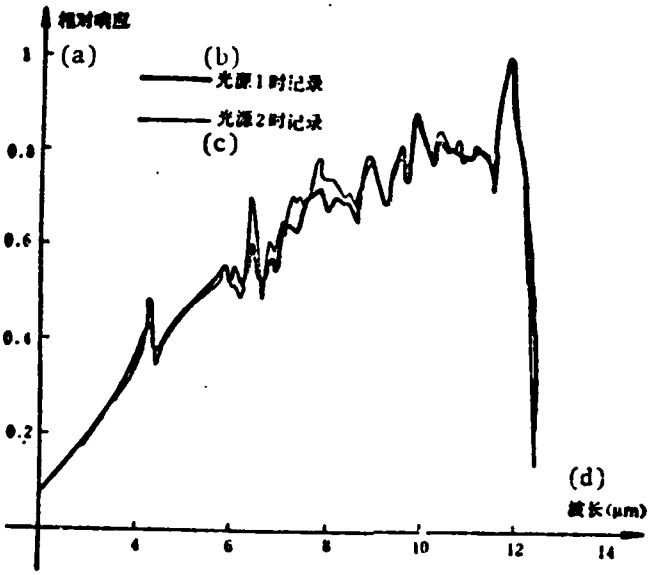

Fig. 5. HgCdTe spectral response curve recorded under different conditions of the light source.
Key: (a) Relative response; (b) Recordings for light source 1; (c) Recordings for light source 2; (d) Wavelength.

of the monochromatic channel at the previous band of the monochromator can be eliminated after comparing both channels. However, in the monochromatic channel, leading out from the monochromator, factors of asymmetry will introduce errors in the measurement.

2. Effect of energy magnitude in measurement

In order to ensure that an amplifier is not saturated when the energy of the light source is at the maximum, the incident energy should be adjusted to an appropriate value. Thus, the energy is correspondingly decreased within the long wave range; as a result, the signal-to-noise ratio is reduced to introduce error in long-wave measurement. An attenuator can be used in the measurement process. However, automatic attenuation will

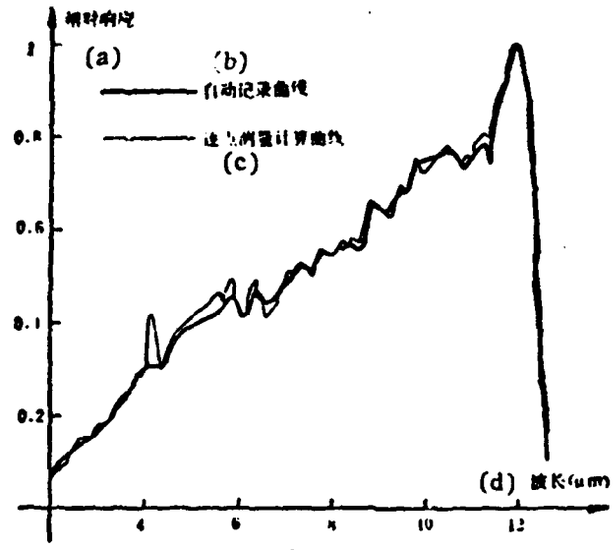

(a) Spectral response of HdCdTe.

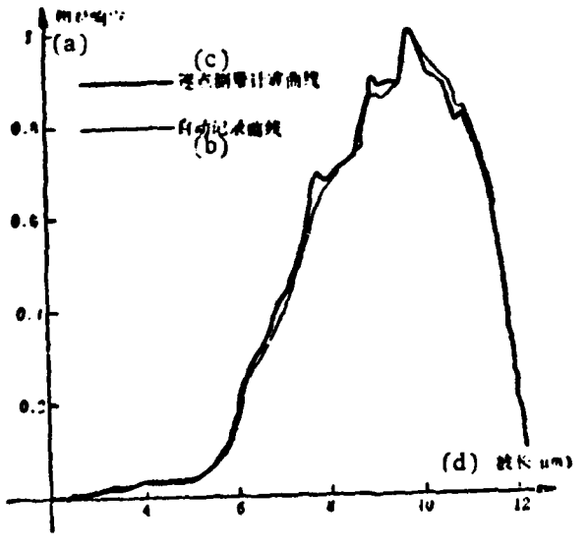

(b) Spectral response of PbSnTe.
Fig. 6. Spectral response curves plotted with automatic recording and with calculation after point-by-point measurement. (Key on following page)

(Fig. 6 continued)
Key: (a) Relative response; (b) Curves plotted with automatic recording; (c) Curves plotted with calculation after point-by-point measurement; (d) Wavelength.

add complexity to the instrument circuit; therefore, automatic change of the slit width can increase input energy in the long wave range in order to ensure measurement accuracy. In selecting the range of slit-width variation, consideration should be given that the emergent light beam has relatively good monochromatic characteristics, not affecting the spectral accuracy during measurement.

3. Spectral error

Since the monochromator displays nonlinear color dispersion in the entire wave band, the wave band with low dispersive power displays less desirable monochromatic characteristics with greater spectral error; this indicates a close relationship with the magnitude of the slit width. A wider slit also causes less desirable monochromatic characteristics. For example, within the range of 0.6 μm~15 μm of a NaCl prism, the dispersive power is greater in the long-wave portion. If the slit width is properly increased, the input energy can be raised. However, the spectral error of the short-wave portion will be comparatively greater. For example, in the vicinity of 3 μm, the linear color dispersion $\Delta\lambda/\Delta\ell$ is approximately 0.308 μm/mm; however, in the vicinity of 12 μm, $\Delta\lambda/\Delta\ell$ is approximately 0.089 μm/mm. Hence, when the slit width is adjusted to 0.5 mm, the spectral error in the vicinity of 3 μm is greater than 0.15 μm. In order to ensure accuracy of spectral measurement, the slit width should be properly selected based on different detector (characteristics). Thus, there will be better monochromatic characteristics in the vicinity of the wavelength concerned (such as peak-value wavelength and cutoff wavelength) to satisfy the requirements of spectral accuracy.

In measurement, selection of measurement speed also affects spectral accuracy. If the speed is too high, the measurement time at each point is smaller than the (circuit) time constant; accurate results are then unable

to be recorded. Therefore, the motor rotational speed should be properly selected based on different color-dispersion conditions of different prisms.

Besides, if there is deviation in adjustment of detector positions, errors in spectral characteristics also can be produced.

The authors express their gratitude to Comrade Xu Shiqiu for his helpful guidance in the research.

LITERATURE

1. Eppeldaner, G., Appl. Opt., 16 (1977), 1, 255.

2. "Procedures for testing infrared detectors and for describing their performances", AD 15759 (1960).

3. Weiladesen (transliteration), R. K., and Bill, A. C., Infrared Detector, translated by Laser and Infrared Compilation Section, National Defense Industry Publishing Service, 1970.

4. Xue Junao, Li Zaiqing, et al., Guangfushe Celiang Yuanli He Fangfa (Principle and Methods of Measuring Photo Radiation), Measurement Publishing Service, 1981.

DESIGN AND ANALYSIS OF INFRARED BROAD-BAND ANTIREFLECTION COATINGS

Xu Buyun
Shanghai Institute of Technical Physics, Chinese Academy of Sciences
Received 4 November 1981

It has been done to optimize an infrared broad-band coating on the theory of equivalent multilayers by means of a computer program named "Random optimization." The practical design and experimental results for 8~14 and 2~14 micrometer wavelength-band on Ge substrate are presented.

I. FOREWORD

In an optical system, it is necessary to have an antireflection feature on optical parts. Broad-band antireflection develops from a single antireflection layer to multiple layers. A very high level of work has been done on the broad-band antireflection scheme in the visible region. On the development of infrared multi-spectrum technique and infrared broad wave band testing and measurement technique, the infrared broad band antireflection work has been more and more stressed. In manuscript (1), studies were made on single layer, double layer, and triple layer antireflection coatings with high refractivity substrate; however, the broad-band work is only limited to 1~7 μm. Later, some researchers worked on antireflection of a four-layer broad band[2] by using highly toxic thallium salt and easily deliquescent fluorides;

in the high transparency band, the antireflection work has been conducted somewhere in the range of 2~10 μm. In recent years, although there were advertisements of better sample curves, there were very few detailed research reports.

Oftentimes, there are shortages of relatively ideal thin coating materials in the broad-band antireflection work of a high refractivity substrate in the infrared region. In the research of this paper, initial coatings were designed based on vector analysis and the concept of equivalent composite coating. Random optimization is utilized to obtain ultrawide coatings in the 2~14 μm wavelength region. In design and experimental manufacture, three types of coating materials were used: Ge, ZnS and SrF_2. These coating materials have relatively good optical, mechanical and anti-deliquescent characteristics with low toxicity and adaptability to the manufacturing process.

II. DESIGN OF INITIAL COATINGS

A general description is given of the design of initial coatings of infrared broad-band antireflection coatings.

1. Vector analysis method

Since generally the refractivity of optical materials used in the infrared region is relatively high, such as $n_{Ge}=4$, and $n_{Si}=3.5$, it is very convenient to determine refractivity of each layer by using the vector analysis method in which the optical thickness of each layer is $\lambda_o/4$ [3].

According to the vector analysis method, we assume that there are k layers of antireflection coatings and the optical thickness of each layer is $\lambda_o/4$ (the phase thickness is 90°). When the refractivity satisfies the following relationship, i.e.:

$$\begin{aligned} n_1^{k+1} &= n_0^k n_2, \\ n_2^{k+1} &= n_0^{k-1} n_2^2, \\ n_3^{k+1} &= n_0^{k-2} n_2^3, \\ &\vdots \\ n_2^{k+1} &= n_0 n_2^{k-1}, \end{aligned}$$

In the equations, n_o is air refractivity and n_k is the refractivity of the k-th layer (k is an integer); then the broad band coating system has k zero reflecting points; the wavelength position is:

$$\frac{k+1}{2k}\lambda_0,\ \frac{k+1}{2(k-1)}\lambda_0,\ \frac{k+1}{2(k-2)}\lambda_0,\ \cdots\cdots,\ \frac{k+1}{4}\lambda_0,\ \frac{k+1}{2}\lambda_0,$$

The width of the lowest reflective point of the obtained broad-band antireflection coating system (the high antireflection region) is $(k+(1/2)k)\lambda_0-(k+1/2)\lambda_0$. The ratio of long wave point to short wave point is k.

Accordingly, in the designed three-layer and five-layer antireflection coating system Ge (wide band and ultrawide band), the optical thickness of each layer is $\lambda_0/4$. From the above-mentioned equation of refractivity and considering some modification of coating materials used, the determined values of refractivity are shown in Table 1. Figures 1 and 2 show the spectral curves.

Table 1. Refractivity values calculated from the vector analysis method.

(a) 层数	折射率 (b) n_1	n_2	n_3	n_4	n_5	(c) 高透射带宽度
3	1.26	2.2	3.1			$0.66\lambda_0-2\lambda_0$
5	1.26	1.65	2.2	2.7	3.3	$0.60\lambda_0-3\lambda_0$

Key: (a) Number of layers; (b) Refractivity; (c) Width of high antireflection band.

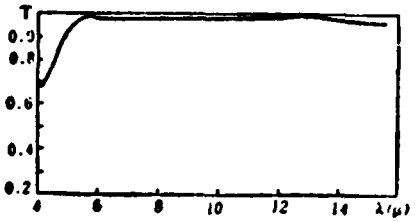

Fig. 1. The calculated transparency curve of a three-layer broad-band antireflection coating system.

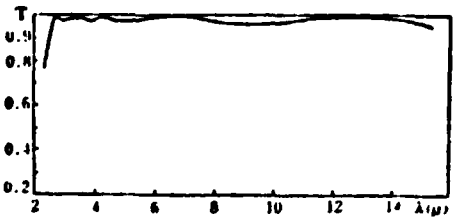

Fig. 2. The calculated transparency curve of a three-layer broad-band antireflection coating system.

2. Usages of symmetrical equivalent composite coating

As previously mentioned, the authors only used three types of coating materials (Ge, ZnS and SrF_2) to complete the design of various broad-band antireflection coating systems; the refractivities of these three materials are, respectively, $n_{Ge}=4$, $n_{ZnS}=2.2$ and $n_{SrF_2}=1.26$. However, in Table 1 the other refractivity values, such as 1.65, 2.7, 3.1 and 3.3, apply the concept of symmetrical composite coating[4]. By using the same method, the refractivities are substituted by equivalent refractivity of the symmetrical equivalent composite coating composed of the three above-mentioned materials.

In the multilayer antireflection design examples of Ge substrate studied by the paper, the third layer ($n_3=3.1$) of the three-layer antireflection syster in Table 1 can be equated with the following symmetrical three-layer structure.

0.2M0.44H0.2M,

in the structure, M represents $ZnS(\lambda_o/4)$ and H represents $Ge(\lambda_o/4)$. We use E and Γ to separately represent equivalent refractivity and equivalent phase thickness of the above-mentioned equivalent composite coating. Then the $E\sim\lambda_o/\lambda$ curve and $\Gamma\sim\lambda_o/\lambda$ curve of the symmetrical composite coating are shown in Fig. 3. From the curve diagram, when the design wavelength $\lambda_o=7.8$ μm, the λ_o/λ value corresponding to 8~14 μm is approximately from 0.55 to 0.97, and the equivalent refractivity lies somewhere within 3.1~3.3. Γ approaches 90^o at $\lambda_o/\lambda=1$. Thus, the equivalent three-layer broad-band antireflection coating system with a Ge substrate including a symmetrical equivalent composite coating is:

Ge|0.2M0.44H1.2ML|A;

in the structure, L represents $SrF_2(\lambda_o/4)$ and A represents air. Obviously, the curve in Fig. 4 can be satisfactorily used to conduct broad-band antireflection design of 8~14 μm.

In the design of the Ge substrate broad band in the paper, in the five-layer ultrawide-band antireflection coatings in Table 1, the parameters ($n_2=1.65$, $n_4=2.7$ and $n_5=3.3$) of the second, the fourth and the fifth layers are equated by the following three-layer symmetrical composite coating:

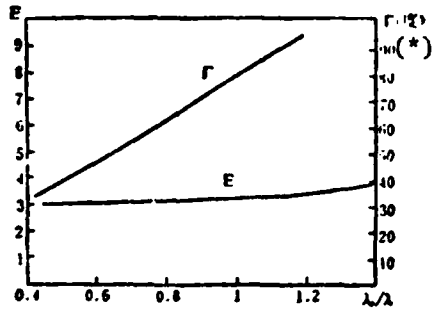

Fig. 3. Curves $E \sim \lambda_0/\lambda$ and $\Gamma \sim \lambda_0/\lambda$ of the symmetrical equivalent composite coating 0.2M0.44H0.2M. Key: *) Degree.

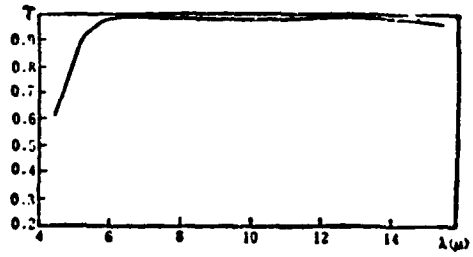

Fig. 4. Calculated spectral transparency curve for design of equivalent three-layer coating Ge|0.2M0.44H1.2ML|A.

$$\frac{(0.24L\,0.48M\,0.24L)}{n_3},$$
$$\frac{(0.36M\,0.24H\,0.36M)}{n_4},$$
$$\frac{(0.22M\,0.54H\,0.22M)}{n_5},$$

Figure 5 shows the curves of Γ and λ_0/λ. Thus, the equivalent five-layer broad-band antireflection coating system (including three equivalent composite coatings) is:

$$\text{Ge}|(0.22M\,0.54H\,0.22M)\,(0.36M\,0.24H\,0.36M)\,M\rightarrow$$
$$(0.24L\,0.48M\,0.24L)\,L|A,$$

After combining, it is an eight-layer coating system:

$$\text{Ge}|0.22M\,0.54H\,0.58M\,0.24H\,1.36M\,0.24L\,0.48M\,1.24L|A,$$

Figure 6 shows the calculated spectral characteristic curve.

Obviously, with the same designed wavelength λ_0 (through calculation in the diagram, λ_0=4.5 μm), the high transparency band of the curve is considerably

narrower in Fig. 6 than in Fig. 2. This is because the equivalent refractivity E value of the $E\sim\lambda_o/\lambda$ curve in Fig. 6 deviates considerably from the designed value (refer to Table 1 for the designed values: n_2=1.65, n_4=2.7 and n_5=3.3).

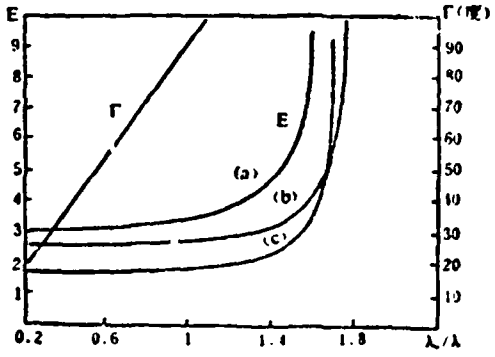

Fig. 5. E, $\Gamma\sim\lambda_o/\lambda$ curves.
Key: *) Degree.

(a) 0.22*M*0.24*H*0.22*M*
(b) 0.36*M*0.24*H*0.36*M*
(c) 0.24*L*0.48*M*0.24*L*

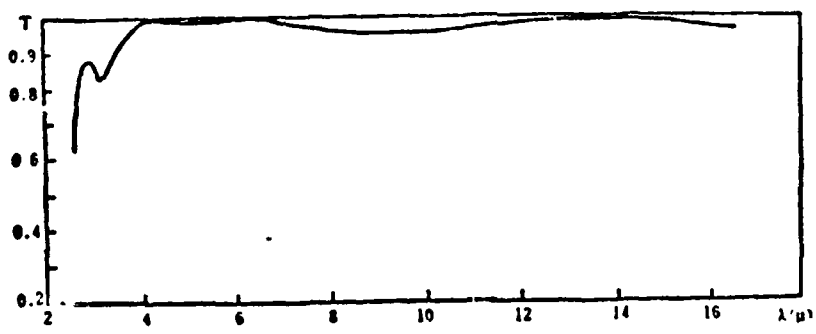

Fig. 6. Experimental spectral transparency curve (taking a cycle for each equivalent coating layer) of equivalent five-layer broad-band antireflection coating system.

III. OPTIMIZATION OF ULTRAWIDE-BAND ANTIREFLECTION COATING SYSTEM BY USING RANDOM OPTIMIZATION

From the analysis in the last section (II), only by using general analysis and trial calculation can relatively satisfactory results be obtained for a broad-band antireflection coating system with not too many layers (such as three layers) when the ultrawide-band antireflection coating system of 2~14 μm is used. While containing three symmetrical equivalent composite coatings with the total number of coatings at 8, the effective antireflection width is significantly reduced when we compare the equivalent spectral curve in Fig. 6 with the curve in Fig. 2. Although the phase thickness of the fundamentally symmetrical structure can be reduced, thus increasing the number of fundamental cycles to improve the spectral curve, yet (by so doing) relatively more layers other than $(\lambda_o/4)$ will exist with smaller phase thickness and difficulty in coating. Hence, by using random optimization[3], the authors considered the above-mentioned eight layers of the coating system as the initial coating system for optimization. Further discussion is needed for using random optimization in automatic design of the coating system. Here, a brief description is given of the basic concept and the application in design of ultrawide band coatings.

We know that generally the refractivity or optical thickness are used as optimization correction parameters of spectral characteristics in optimization design of coating systems. In the selective conditions of refractivity and other conditions, the refractivity R of a group of coating systems can be expressed by using the following function forms:

$$R=R(X_1, X_2, \ldots, X_n, \lambda).$$

In the equation, $X_1, X_2, \ldots, X_n$ are optical thicknesses of various layers; n is an integer. As expressed by the above equation, R is an n-dimensional space function. If at a certain point:

$$X^*(X_1^*, X_2^*, \ldots, X_n^*)$$

of an n-dimensional space, there is an ideal R value; this point X* is the optimized target value. The process of thin-coating automatic design of random optimization is: beginning from parameters of initial design of a point

$X^0(X_1^0, X_2^0, \ldots, X_n^0)$ in the above-mentioned n-dimensional space, within the specified variation range of parameters (of various layers), along a randomly selected direction and step length to point X', continue to move forward if R becomes smaller. If R becomes greater, reverse the direction and move forward with the same step length. If R becomes smaller, move forward along the same direction. If R becomes greater, select a new direction and step length. Continue like this. In order to derive the minimum value of R, and to have R varied from a local minimum to a "remoter" minimum value, the randomly selected direction and step length can be divided by the same constant C. In the optimization process, the magnitude of C can be controlled with acceleration of step length. In computer calculation, C varies from small to large until a relatively satisfactory result can be designed; i.e., the corrected parameter X can be made to gradually approach X^* from X^0 in order to obtain a satisfactory R value. In the optimization process, if the initial parameters are not used, the middle points of the specified variation range of various parameters can be used as initial points. Continue the optimization according to the above-mentioned process.

To design a 2~14 μm ultrawide antireflection coating system, while only using the coating system of three coating materials (Ge, ZnS and SrF_2) and eight-layer (total number of layers) coating, the spectral characteristic curves are not ideal. Thus, the authors used the eight-layer coating system as the initial structure, prescribing to conduct optimization during vertical incidence in the wavelength region 2.2 μm≤λ≤13.4 μm. In the optimization process, the authors selected a mode of maximum value

$$F=\max R(\lambda_i) \quad (1\leq i\leq M)$$

as the evaluation function; M is the number of wave points. Table 2 shows the optical thicknesses of various layers before and after optimization. Figure 7 shows a calculated spectral characteristic curve of the eight-layer coating system after optimization. In the above-mentioned wavelength region, the maximum point $R_{max}=0.024$ after optimization. It can be seen that the spectral curve of the initial eight-layer coating system is significantly improved for post-random-optimization eight-layer coating. Thus, in the 2~14 μm spectral

region, there will be a higher antireflection characteristic; this sufficiently reveals the function of random optimization in optimization of an optical coating system.

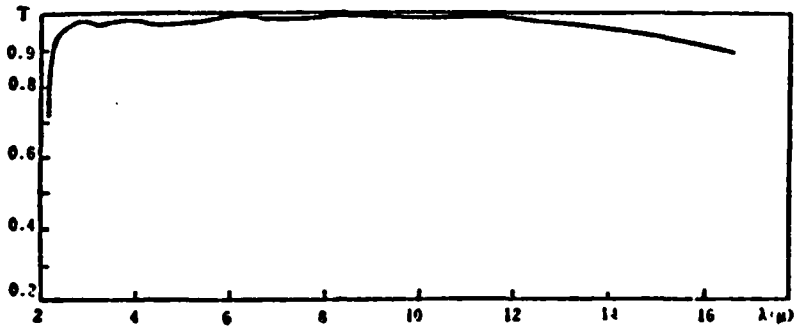

Fig. 7. Calculated spectral curve (n_s=4) of eight layers after optimization

Table 2. Eight layer thickness parameters (unit: $\lambda_o/4$) before and after optimization.

	X_1	X_2	X_3	X_4	X_5	X_6	X_7	X_8
(a)优化前	1.24	0.48	0.24	1.36	0.24	0.58	0.54	0.22
(b)优化后	1.2	0.19	0.265	1.347	0.114	0.536	0.848	0.218

Key: (a) Before optimization; (b) After optimization.

As mentioned above, the T~λ curves were calculated by considering only the antireflection effect of a single surface of the base plate. It is assumed that another surface extends without a limit. In the following, the given experimental results are results when both surfaces of the base plates are covered with the same coating system.

IV. EXPERIMENTAL RESULTS AND ANALYSIS

On ordinary optical multilayer equipment (DMD-450) controlled by comparison-plate harmonics, the authors used a non-($\lambda_0/4$) control curve[4] to control the optical thickness of various layers. It is not too difficult to coat a practical broad-band antireflection coating system. Characteristics vary somewhat in repeated tests; however, the transparency level is basically the same in each experimental curve. Figure 8 shows the spectral characteristic curves during an experiment on an equivalent three-layer broad-band antireflection coating system with 4 as the total number of layers. Figure 9 shows the spectral characteristic curves of an 8-layer ultrawide coating system after optimization.

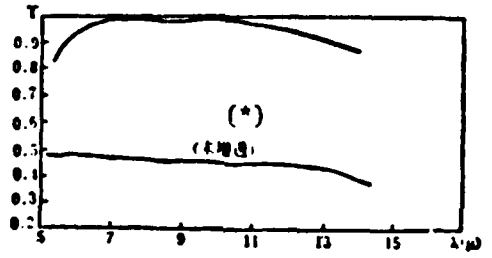

Fig. 8. Experimental curves (double surfaces) of equivalent three-layer broad-band antireflection coatings.
Key: *) (without antireflection).

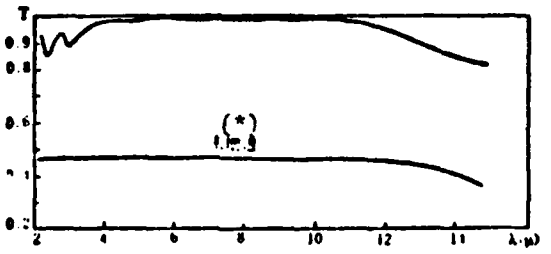

Fig. 9. Experimental curves (double surfaces) of eight-layer broad-band antireflection coatings obtained by using random optimization.
Key: *) Without antireflection.

Although the experimental curves shown in Fig. 9 have better antireflection characteristics, the deviation is somewhat clear compared with the calculated value. This deviation is due to two reasons: (1) The theoretical calculation does not consider color dispersion and absorption of materials within a very wide wavelength range. There are some absorptions following 13 μm by Ge, ZnS and SrF_2; there is the effect of the water absorption band in the vicinity of 3 μm. (2) Errors in the non-($\lambda_0/4$) point controlled by the coating control instrument for an ordinary photoelectrode value are relatively great, so that the experimental curve does not have a good match with the calculated value.

Although there are some difficulties in experiments, the following characteristics correspond to the merchandise index of the OCLI Company of the United States: broad-band antireflection curves of Ge substrate within the range of 8~14 μm and 2~14 μm, average transparency, and transparency of the lowest point. The average transparency used in the broad-band transparency curve (8~14 μm) within 8~12 μm is $\overline{T}_{2.5\ 14}$=94.6 percent; the transparency (of the lowest point) is T_{min}=82.5 percent.

Although some other materials can be found in the 2~14 μm wavelength region to satisfy the requirements of some layers in broad-band antireflection, and to possibly show some better spectral characteristics, yet viewed from practical applications, materials (easily deliquescent, soft coating, and high toxicity) are unfavorable for manufacture and usage. Hence, the authors selected the relatively appropriate materials (Ge, ZnS, and SrF_2) as coating materials. Although there were some additional difficulties in design and manufacture, design and manufacture problems for wide bands (8~14 μm and 2~14 μm) are being solved better.

In principle, the design concept described in the paper is also suitable to design and manufacture broad-band antireflection coating systems of other high refractivity substrates.

The author expressed his gratitude to Tao Fengxiang, Zhu Furong, et al. for their assistances in design and manufacture for the study.

LITERATURE

1. Young, L., J. Opt. Soc. Am., 51 (1961), 967.

2. Church, E. L. et al., Appl. Opt., 13 (1974), 1274.

3. Macleod, H. A., Thin-Film Optical Filters, London: Adam. Hilger. Ltd., 1969. Chinese translation: Guangxue Bomo Jishu (Optical Thin Coating Technique), translated by Zhou Jiulin and Yin Shubai, National Defense Industry Publishing Service, 1974.

4. Berning, P. H., J. Opt. Soc. Am., 52 (1962), 431.

5. Tao Fengxiang, Hungwai Wuli Yu Jishu (Infrared Physics and Technique),(1978), 4, 49.

6. Zhang Fengshan, Hungwai Wuli Yu Jishu, (1975), 3, 1.

CHINESE JOURNAL OF INFRARED RESEARCH

紅外研究

1(1982), 1, 21~28

红外研究
Chin.J.Infrared.

红外探测器光谱响应自动测量

林　林、牟樊南、孙健邦、吴冰洁

（中国科学院上海技术物理研究所）

摘要——本文主要阐述红外探测器光谱响应自动测量的方法，扼要地介绍了测试系统及其性能、测量原理和系统设计。测量结果表明，这套系统能消除光源和环境变化的影响，提高测量的精度和速度。

一、引　言

红外探测器光谱响应是红外探测器的主要特性之一，它描述了探测器响应率与波长的关系。探测器的响应率随波长变化的曲线是系统设计的主要依据之一。

过去，红外探测器相对光谱响应的测量一般在单色仪上进行，采用逐点测量的方法。红外光源经过调制后，进入单色仪分光，得到调制的单色光，先用无选择性的热探测器，例如真空热电偶，热释电探测器等进行接收，得到一组随波长变化的电输出数据，再由被测探测器进行接收，同样得到一组数据，将这两组数据一一对应进行比较，就可计算出一组被测探测器的光谱响应数据。这种方法比较繁琐，不但花费的时间较多，而且由于两组数据不是同时测量，光源的不稳定性，测量设备的不稳定性和测量过程中环境的变化等都会给测量带来较大的误差。

为了方便、准确而又迅速地得到红外探测器光谱响应曲线，我们改进了测量方法，即采用实时比较测量方法，把单色仪出射狭缝出来的光，用光学系统分成两束，一束光由热探测器接收，另一束光由被测探测器接收，把这两个探测器同时接收到的信号进行比较，经过比率计处理就能直接自动记录下红外探测器的等功率光谱响应曲线。实验结果表明，这样记录下来的等功率光谱响应曲线能消除光源的不稳定性和环境变化的影响。提高测量精度和速度。

二、测量的基本原理

在调制单色光源的作用下，参考探测器输出的电动势 $V_m(\lambda)$ 与光源的光谱功率分布 $\phi(\lambda)$、单色仪的仪器函数 $N(\lambda)$、单色仪的透射比 $\tau(\lambda)$，以及参考探测器本身的光谱响应 $G_m(\lambda)$ 成正比，即：

本文 1981 年 11 月 19 日收到。

$$V_{sR}(\lambda) \propto \phi_1(\lambda) N_1(\lambda) \tau_1(\lambda) G_{sR}(\lambda), \tag{1}$$

在同样的条件下，被测探测器输出的电动势 $V_s(\lambda)$ 类似地为：

$$V_s(\lambda) \propto \phi(\lambda) N(\lambda) \tau(\lambda) G(\lambda), \tag{2}$$

其中 $G(\lambda)$ 为被测探测器本身的光谱响应。

比较上述两式并整理后得：

$$G(\lambda) = \frac{G_{sR}(\lambda) V_s(\lambda)}{V_{sR}(\lambda)}. \tag{3}$$

如果 $G_{sR}(\lambda)$ 是与波长无关的常数，则只要测量出 $V_s(\lambda)$ $V_{sR}(\lambda)$，就可得出探测器的相对光谱响应，我们研制的装置就是根据这样的原理做成的(对于 $G_{sR}(\lambda)$ 的修正问题，本文暂不作讨论)。测量装置原理见图 1。

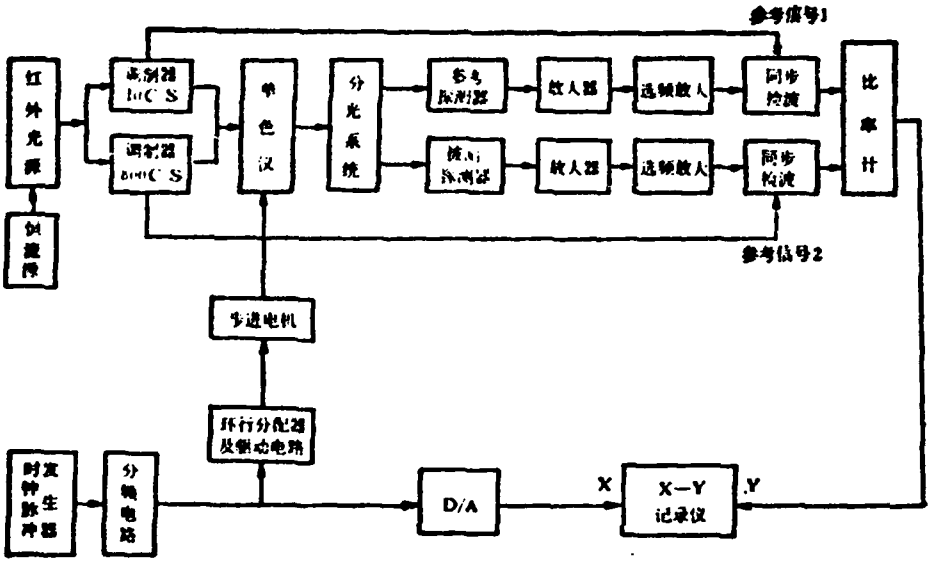

图 1　自动测量装置原理图

红外光源聚焦后分成上下两路，分别调制成两种不同的频率，经过单色仪分光，得到两种调制频率的单色光束，再将不同调制频率的光束分成两路，分别被参考探测器和被测探测器接收。经过放大，相敏检波后，将两个探测器同时接收到的能量信号在比率计上相除，并且将单色仪棱镜转动和绘图仪的 X 笔同步，就可以连续画出被测探测器相对光谱响应曲线。

三、系统设计

仪器由光学系统，信号处理系统，波长扫描系统和绘图仪等几部分组成。

1. 光学系统

光学系统包括光源，调制器，单色仪和分光系统，如图 2 所示。

我们用能斯特灯源作为红外光源，它在较宽波段上均有辐射。光源的工作电流由稳流源提供，光源的工作电流连续可调，一般工作在 0.6 A。

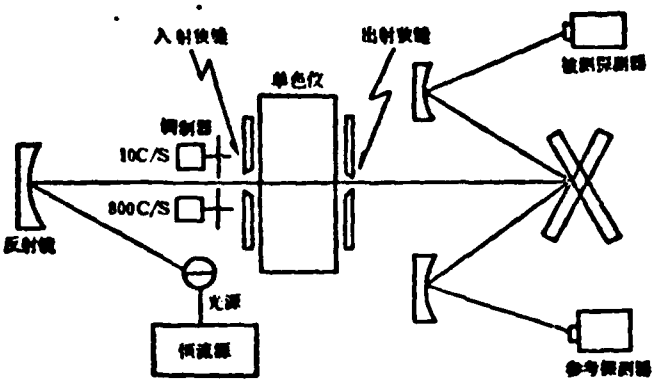

图2 光学系统原理图

能斯特光源经反射镜聚焦以后，光束落在单色仪的入射狭缝上，形状是狭长的。机械调制装置放置在光源和单色仪入射狭缝之间，在光束上下各取一半进行调制。每个调制盘的两边都分别装有一个小灯泡和硅光电二极管，调制盘转动时，同时调制小灯泡的光，使硅光二极管接收到调制盘的同步信号，用来作为相敏检波的参考信号，以便得到较大的信噪比。调制频率取决于探测器，如果参考探测器采用 TGS 热释电器件，被测探测器为光电型探测器，则根据这两类器件的特点，调制频率分别取为 10C/S 和 800C/S。

单色仪采用 Carl Zeiss SPM-2 型单色仪。根据被测探测器光谱响应的要求，采用相应的棱镜进行分光，波长扫描由步进电机带动。

从单色仪出射狭缝出来的 10C S 和 800C/S 上下两束调制的单色光，分别落在交叉成 45° 的上下两块平面镜上，由两块平面镜分别反射到对应的两块凹面镜上，聚焦在参考探测器和被测探测器的响应元上。这样，两个探测器同时接收到同一个光源的信号 如果两个光路上反射镜的反射特性基本一致，则两个光路上光束的单色性是一致的，而其能量大小之比在整个测量的光谱范围内是不变的。所有的光学元件和探测器都安装在三轴可调的微调架上，便于测量时精确地调整其位置。

2. 信号处理系统

信号处理系统包括信号接收电路和比率计两个部分。

参考探测器和被测探测器采用两个相应的不同的前置放大器进行弱信号检测，经两路主放大器和 R-C 选频放大器，分别进行放大和选频。选频放大器的中心频率与相应的调制频率一致，放大器具有较宽的动态范围，对整个光谱波段上接收到的能量信号，放大器具有固定的增益。为了提高电路检测信号的能力，采用了鉴相器原理，分别对信号进行了相敏检波，将探测器接收到的交流信号转变为直流信号，供比率计作信号处理。相敏检波的参考信号由调制盘上的硅光二极管输出，为了调整参考信号和接收信号之间的相位关系，电路中设计了可调移相电路，分别对两路参考信号进行相位调整。整个电路的时间常数主要取决于相敏检波的积分时间 τ，为取得较好的相敏检波效果，积分时间选为 2.5 秒，两路的时间常数相等。

比率计是这台仪器的关键，为了使电路结构简单，采用模拟除法器来实现比率的要求。利用对数电路原理组成除法器电路，其数学表达式如下：

$$V_o = \text{Antilog}(\log x - \log y) = x/y. \quad (4)$$

自锁相除法器电路中，用四只运算放大器组成对数和反对数电路，只要在四个反馈晶体管相互匹配的条件下，运算精度和温度稳定性都是比较理想的，在输出范围内的运算精度在2%之内。

从相敏检波出来的两路信号同时送到比率计的输入端，被测探测器的信号作为分子，参考探测器的信号作为分母，在分子或分母发生变化时，比率计能正确地测量出瞬时比值。将比率计输出的比值信号加到记录仪的Y笔上，就可以记录下相对光谱响应的曲线。当光源或其他因素引起分子分母同时按比例变化时，比率计输出不变。这就可能消除光源变化、环境温度和空气组份变化引起的误差。

3. 波长扫描系统

波长扫描系统包括步进电机，驱动电路，*D/A* 转换电路和记录笔限位等继电器联动电路。

单色仪波长扫描由步进电机带动，我们将步进电机直接和单色仪上的波长调节手轮相连。电机的步距为1.5°，单色仪中心波长从0.6 μm～15 μm 变化，电机需转动约3600步。对于NaCl棱镜，色散较小的是在2 μm～3 μm 之间，每隔0.1 μm，步进电机转动8～9步，因此步进电机的步距能满足波长的精度0.1 μm 的要求。

电机的转速是这样考虑的，设信号处理电路的时间常数为 [redacted] 当电机转动速度足够慢时，就能保证在电路时间常数几倍的时间内充分记录每一波长相应的比率计输出。为了有效地提高测试速度，我们确定每一波长所需测试时间为 [redacted] 如果隔0.1 μm 测一个点，则在光色散最小区域，波长扫描0.1 μm 时，步进电机转动 N 步所需的时间为 [redacted] 则步进电机的频率为 $N/$ [redacted]

根据不同探测器对测试波长精度的不同要求，可选取不同的记录速度，我们目前选取的电机时钟频率分别为1 Hz, 2 Hz, 4 Hz 三种，由时钟脉冲进行分频后供给，从0.6 μm～15 μm 记录时间分别为15 min, 30 min, 60 min。从2 μm～14 μm 记录时间分别为11 min, 21 min, 42 min 等。

为了使系统简单、可靠，避免由于时钟频率不稳带来的误差，采用同一时钟为基准，同步驱动棱镜转动和记录仪X笔同步工作。时钟脉冲进行分频后分为两路，一路通过环行分配器和功率放大电路驱动步进电机旋转；另一路输入数模转换电路，把时钟脉冲转换为记录仪上X笔的直流信号。这是一个高阶数、长时间的阶梯积分电路，积分时间长达几十分钟，阶数高达3600阶以上，每阶不到1 mV。因此，加在X笔上的是随时间变化按比例上升的直流电压，其线性度优于1%。

由于棱镜色散的非线性，记录纸的光谱刻度必须专门对应棱镜的色散刻度进行标定，这样记录的光谱误差小于0.1 μm。如果X笔不加电压，也可以让记录纸移动，采取人工打点的方法来标定波长坐标。

四、测量结果

我们对几种不同类型的光电探测器进行了多次测量，测量的结果表明，该系统能够有效地对探测器的光谱响应进行测试。

1．改变光源的工作电流(分别调在0.6A和0.9A)进行测量，被测探测器的相对光谱响应基本一致，见图3。我们又在不同时间测试了两个能斯特灯的分谱辐射曲线，这两根曲线是不重合的，见图4。但对同一探测器进行相应的两次测试，响应曲线是比较接近的，见图5。这说明该系统对于消除测量过程中光源变化的影响是有效果的。

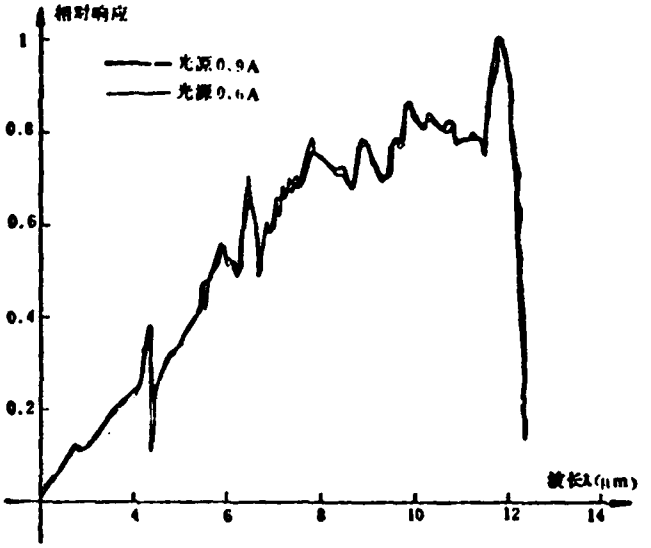

图3　光源在不同工作电流时，HgCdTe探测器的光谱响应曲线

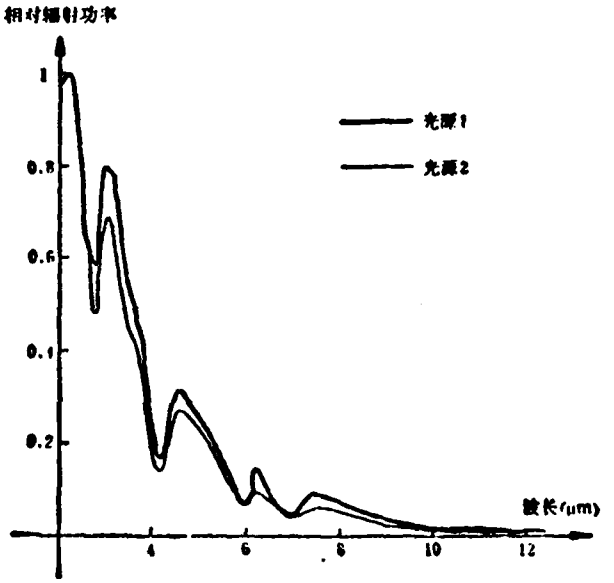

图4　两个不同光源的辐射曲线

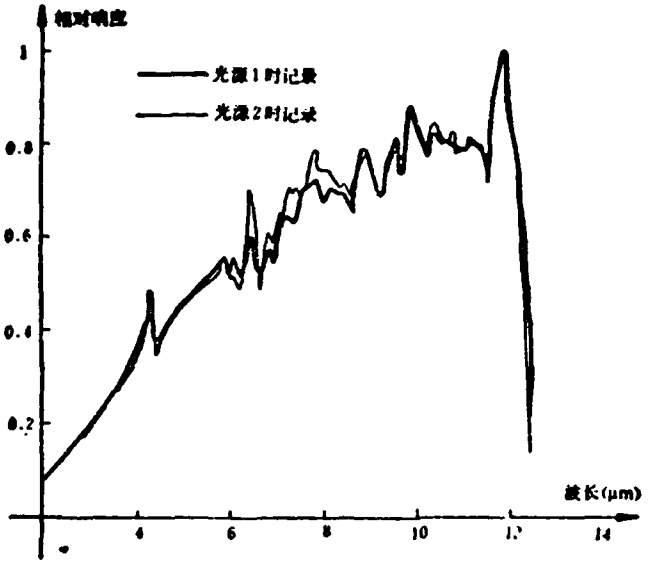

图5 不同光源条件下记录的HgCdTe光谱响应曲线

2. 将自动测量所得的曲线与同一探测器逐点测量后计算作出的光谱响应曲线相比，峰值波长与截止波长基本相符，曲线形状基本相同，见图6(*a*)和(*b*)，而测试速度要快十几倍。

3. 根据被测探测器和参考探测器的性能特点选择几个不同的波段，在一定范围内改变单色仪狭缝宽度，比率计输出的数据基本一致，说明狭缝改变时，虽然引起能量变化，但由于两路信号实时比较，分子和分母如以同样比例改变，其结果不变。如表1所示。

表1 狭缝改变时的比率计输出

输入狭缝宽度 / 波长	0.5mm	0.4mm	0.3mm	0.2mm
5μm	0.67 V	0.67 V	0.67 V	0.67 V
10μm	1.5 V	1.5 V	1.5 V	1.5 V

五、测量误差分析

1. 环境影响

由于所测探测器的响应波段一般在2μm～15μm之间，因此周围温度的变化和大气组份的变化都会给测量带来误差。对于单色仪前一段光路上的变化，经两路比较可以消除，但在单色仪以后的单光路上，不对称因素就会给测量带来误差。

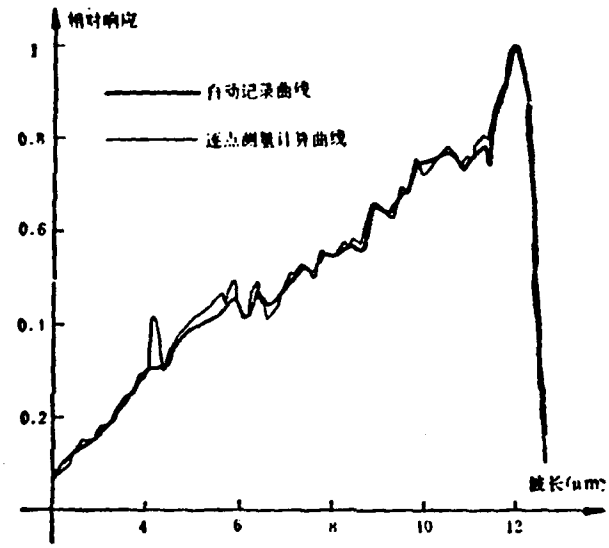

(a) HgCdTe的光谱响应

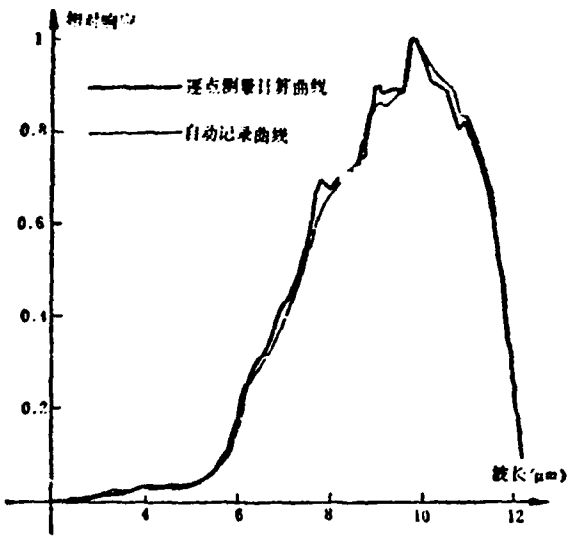

(b) PbSnTe的光谱响应

图6 自动记录和逐点测量后计算的光谱响应曲线

2. 测量中能量大小的影响

为了保证放大器在光源能量最大时不至于饱和，就必须将入射能量调至适当值，这样在长波范围能量相应减少，以至信噪比降低，给长波的测量带来误差。可在测量过程中采用衰减器，但自动衰减会使仪器电路复杂化，因此可以通过自动改变狭缝宽度来增加长波范围内输入能量，以保证测量的准确性。但狭缝宽度变化的选择范围，必须考虑到出射的光束具有较好的单色性，不能影响测量的光谱精度。

3. 光谱误差

由于单色仪本身在整个波段的色散是非线性的，在色散率小的波段单色性较差，光谱误差比较大，这与狭缝的大小有密切的关系。狭缝增大也会引起单色性变差，如 NaCl 棱镜 0.6 μm～15 μm 中，长波部分色散率较大，如使狭缝宽度适当增大，可以提高输入能量，但短波部分的光谱误差就会比较大。例如在 3 μm 附近，线色散 $d\lambda/dl$ 约为 0.308 μm/mm，而在 12 μm 附近 $d\lambda/dl$ 约为 0.089 μm/mm，因此当狭缝调节在 0.5 mm 时，3 μm 附近的光谱误差就要大于 0.15 μm。为了保证光谱的测量精度，必须根据不同的探测器，正确选择狭缝宽度，使所关心的波长（如峰值波长和截止波长）附近具有较好的单色性，以满足光谱精度的要求。

在测量中，对测量速度的选择也影响光谱的精度，如速度太快，每点测量时间小于电路的时间常数，就不可能记录出正确的结果。因此必须根据不同棱镜不同的色散情况来正确选取电机转动的速度。

此外，探测器位置调整若有偏差，也会产生光谱特性的误差。

致谢 本工作得到徐世秋同志的有益指导，谨表示感谢。

参 考 文 献

[1] G. Eppeldauer, *Appl. Opt.*, **16** (1977), 1, 255.
[2] "Procedures for testing infrared detectors and for describing their performance". AD 15759(1960).
[3] R. K. 威拉德森，A. C. 比尔，红外探测器，激光与红外编辑组译，国防工业出版社，1970.
[4] 薛君敖，李在清等，光辐射测量原理和方法，计量出版社，1961.

AUTOMATIC MEASUREMENT OF SPECTRAL RESPONSE OF INFRARED DETECTORS

LIN LIN, MU XIERUN, SUN JIANBANG, WU BINJIE
(Shanghai Institute of Technical Physics, Academia Sinica)

ABSTRACT

The method of automatic measurement of the spectral response of infrared detectors is discussed. A special system has been built and its performances tested. The principle of the measurement and the design of the system are presented. The results show that a number of problems generally encountered in such measurements can be eliminated.

1(1982), 1,71~76

红外研究
Chin.J.IR Res.

红外宽带增透膜系的设计与分析

许步云

(中国科学院上海技术物理研究所)

摘要——依据等效多层膜的概念设计了红外宽带增透膜系，利用一种膜系自动设计的方法——随机优选法——对宽带膜系实现最优化。提供了锗衬底在8~14 μm 和 2~14 μm 波长区的设计实例与实验结果。

一、引　言

光学系统中，对光学零件的增透工作是必不可少的。宽带增透的要求，使增透层从单层发展到多层。可见区的宽带增透工作已做出很高的水平。随着红外多光谱技术及红外宽波段检测技术的发展，为提高光学系统的效率，红外宽带增透工作也日益受到重视。文献[1]对高折射率衬底的单层、双层及三层增透膜作了研究，但是宽带工作也仅限于 1~7 μm之间。后来有人做过四层宽带增透工作[2]，用了毒性较大的铊盐和易潮解的氟化物，高透射带也仅做到 2~10 μm 之间。当然，近几年虽有更好一些的样品曲线广告，但是具体研究报道甚少。

红外区高折射率衬底的宽带增透工作往往缺少比较理想的薄膜材料。在本文工作中，依据矢量分析和对称等效组合膜概念设计了初始膜系，并用"随机优选法"获得工作于 2~14 μm 波长区的超宽膜系。在设计和实验制作中使用了三种膜料：Ge、ZnS、SrF_2，这些膜料有较好的光学性能、机械性能及抗潮解性能，而且这三种膜料毒性小，工艺又较易实现。

二、初始膜系的设计

下面将对红外宽带增透膜的初始膜系设计作一概述。

1. 矢量分析法

由于红外区使用的光学材料的折射率一般比较高，如 $n_{Ge}=4$，$n_{ZnS}=3.5$ 等。因而红外宽带增透膜系的各层折射率可以采取从衬底向空气逐渐过渡的方式，而用各层光学厚度都为 $\lambda_0/4$ 的矢量分析法确定各层折射率是很方便的[3]。

根据矢量分析法，设有 k 层增透膜，每层光学厚度为 $\lambda_0/4$(相位厚度为 90°)，当折射率满足下列关系时，即：

本文 1981年 11 月 4 日收到。

$$n_1^{k+1} = n_1^k n_0,$$
$$n_2^{k+1} = n_2^k n_0^2,$$
$$n_3^{k+1} = n_3^k n_0^3,$$
$$\vdots$$
$$n_k^{k+1} = n_k^k n_0^{k-1},$$

其中，n_0 是空气折射率，n_k 是第 k 层折射率（k 为整数），则此宽带膜系就有 k 个零反射点，所在波长位置为：

$$\frac{k+1}{2k}\lambda_0,\ \frac{k+1}{2(k-1)}\lambda_0,\ \frac{k+1}{2(k-2)}\lambda_0,\ \cdots\cdots,\ \frac{k+1}{4}\lambda_0,\ \frac{k+1}{2}\lambda_0,$$

所得宽带增透膜系的最低反射点宽度（即高增透区域）为 $(k+1/2k)\lambda_0-(k+1/2)\lambda_0$，长波点与短波点之比为 k 倍。

据此，为[illegible]衬底设计三层和五层的宽带和超宽带增透膜系，每层光学厚度为 $\lambda_0/4$。由上述折射率的关系式并考虑到所用膜料而稍加修正所确定的折射率值见表 1。光谱曲线由图 1 和图 2 所示。

表 1　矢量分析法计算的折射率值

层数 \ 折射率	n_1	n_2	n_3	n_4	n_5	高透射带宽度
3	1.26	2.2	3.1			$0.66\lambda_0-2\lambda_0$
5	1.26	1.65	2.2	2.7	3.3	$0.60\lambda_0-3\lambda_0$

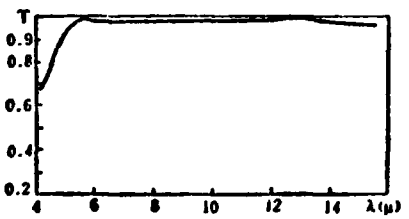

图 1　三层宽带增透膜系的计算光谱透射曲线

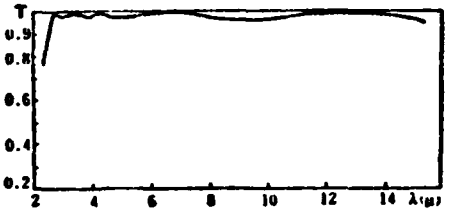

图 2　五层宽带增透膜系的计算光谱透射曲线

2. 对称等效组合膜的运用

前面说过，我们仅用三种膜料（Ge、ZnS、SrF_2）完成各宽带增透膜系的设计，这三种材料的折射率分别为 $n_{Ge}=4$，$n_{ZnS}=2.2$，$n_{SrF_2}=1.26$。而表 1 中的其余折射率值诸如 1.65，2.7，3.1，3.3 等都根据对称组合膜的概念[4]，用同样方法以上述三种材料所构成的对称等效组合膜的等效折射率代之。

在本文所考察的[illegible]衬底多层增透设计实例中，表 1 中三层增透膜系中的第三层（$n_3=3.1$）可用如下对称三层结构等效之：

$$0.2M\,0.44H\,0.2M,$$

其中，M 代表 ZnS（$\lambda_0/4$），H 代表 Ge（$\lambda_0/4$）。用 E 和 Γ 分别表示上述对称等效组合膜的等效折射率和等效相位厚度，则该对称等效组合膜的 $E\sim\lambda_0/\lambda$ 曲线和 $\Gamma\sim\lambda_0/\lambda$ 曲线由图 3 所示。从曲线图上可以看出，当设计波长 $\lambda_0=7.8\,\mu m$ 时，对应于 8～14 μm 的 λ_0/λ 值约从

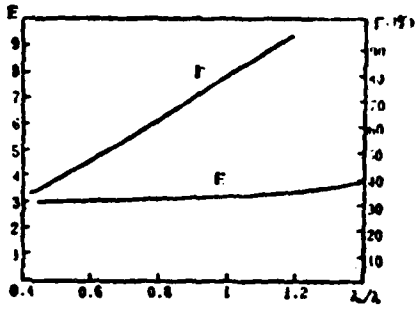

图3 对称等效组合膜 $0.2M0.44H$ $0.2M$ 的 E, $\Gamma\sim\lambda_0/\lambda$ 曲线

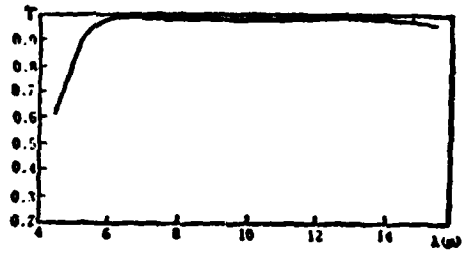

图4 设计等效三层膜 $Ge|0.2M0.44H$ $1.2ML|A$ 用的计算光谱透射曲线

0.55到0.97，等效折射率在3.1~3.3之间。在 $\lambda_0/\lambda=1$ 处 Γ 接近90°。这样，包含一个对称等效组合膜的Ge衬底等效3层宽带增透膜系为：

$$Ge|0.2M0.44H1.2ML|A,$$

其中，L 代表 $SrF_2(\lambda_0/4)$，A 代表空气。显然，图4的曲线已能很好地用来作8~14 μm的宽带增透设计。

在本文Ge衬底宽带设计中，表1中五层超宽带增透膜系之第2，4，5各层参数（$n_0=1.65$，$n_H=2.7$，$n_L=3.3$）各用如下的三层对称组合膜等效之：

$$\frac{(0.24L0.48M0.24L)}{n_0},$$

$$\frac{(0.36M0.24H0.36M)}{n_H},$$

$$\frac{(0.22M0.54H0.22M)}{n_L},$$

Γ 与 λ_0/λ 关系曲线由图5表示。这样，包含三个等效组合膜的等效五层宽带增透膜系为：

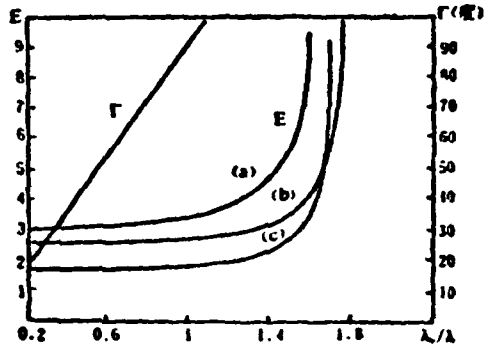

图5 E, $\Gamma\sim\lambda_0/\lambda$ 曲线
(a) $0.22M0.24H0.22M$
(b) $0.36M0.24H0.36M$
(c) $0.24L0.48M0.24L$

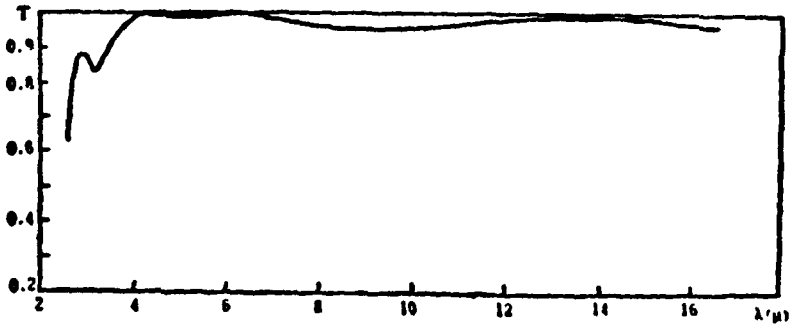

图6 等效五层宽带增透膜系（总数为八层）实验光谱透射曲线（每个等效膜层都取一个周期）

$$Ge|(0.22M\,0.54H\,0.22M)^{\wedge}(0.36M\,0.24H\,0.36M)M\rightarrow$$
$$(0.24L\,0.48M\,0.24L)L|A,$$

合并后为八层膜系.

$$Ge|0.22M\,0.54H\,0.58M\,0.24H\,1.36M\,0.24L\,0.48M\,1.24L|A,$$

计算光谱特性曲线见图 6。

显然，在相同的设计波长 λ_0(图中计算取 $\lambda_0=4.5\mu m$)，曲线的高透射带在图 6 中比图 2 中要窄得多。这是因为图 6 的 $E\sim\lambda_0/\lambda$ 曲线，在 λ_0, $\lambda\geqslant1.2(\lambda<3.7\mu m)$时，等效折射率 E 值偏离设计值较大。(设计值见表 1: $n_3=1.65$, $n_4=2.7$, $n_5=3.3$)。

三、"随机优选法"对超宽带增透膜系的最优化

从上节分析可以看出，对层数不太多(如三层)的宽带增透膜系，只须用一般的分析与试算就可获得比较满意的结果。而用于 2～14 μm 的超宽带增透膜系，当包含三个对称等效组合膜，总层数为八层时，图 6 等效光谱曲线与图 2 曲线相比，有效增透宽度显著缩小。虽然可以采取缩小基本对称结构的相位厚度，从而增加基本周期数来改善光谱曲线，但这样做就会存在较多的非 $\lambda_0/4$ 层，并且相位厚度较薄，镀制困难。为此，我们把上述八层膜系作为初始膜系进行最优化，使用的方法是"随机优选法"[8]。关于"随机优选法"在膜系自动设计中的运用有待进一步讨论，这里仅将其基本思想及其在超宽膜设计中的运用作一扼要描述。

我们知道，在膜系的最优化设计中，通常或是把折射率，或是把光学厚度作为光谱特性最优化的校正参数。若在折射率及其他条件都选定的情况下，一组膜系的反射率 R 可以用下列函数形式表示:

$$R=R(X_1, X_2, \cdots, X_n, \lambda)$$

式中 X_1, X_2, …, X_n 是各层光学厚度，n 为整数。上式表示，在给定的波长上，R 是一个 n 维空间函数。如果在 n 维空间某一点:

$$X^*(X_1^*, X_2^*, \cdots, X_n^*),$$

有理想的 R 值，则此点 X^* 为最优化的目标值。作为随机最优化的薄膜自动设计，其过程是: 从上述 n 维空间中某一点 $X^0(X_1^0, X_2^0, \cdots, X_n^0)$ ——初始设计的参数出发，在各层参数规定的变化范围内，沿随机选取的方向和步长到 X' 点，若 R 变小，则继续前进；若 R 变大，则沿相反方向以同一步长前进，若 R 变小，就继续前进，若 R 变大，那么重新选取方向和步长，依此类推。为了求得 R 的极小值，并使 R 从某个局部极小跳到"较远"极小值，可以对随机选取的方向和步长同除一个常数 C，在优化过程中可以控制 C 的大小，并加有步长加速措施。在电子计算机计算中 C 反复从小到大变化，一直到设计出较满意的结果，亦即使得校正参数 X 从 X^0 逐步逼近到 X^*，以获得满意的 R 值。在最优化过程中，若不用初始参数，也可以用各参数被规定的变化范围的中点作为初始点，按上述程序不断调优。

为设计 2～14 μm 超宽增透膜系，当仅使用 Ge, ZnS, SrF_2 三种膜料而总层数为八层膜的膜系时，光谱特性曲线是很不理想的。为此我们把这样的八层膜系作为初始结构，规定在波长区 $2.2\mu m\leqslant\lambda\leqslant13.4\mu m$，垂直入射时进行最优化。在优化过程中，我们选取最大值模

$$F=\max R(\lambda_i)$$
$$(1\leqslant i\leqslant M)$$

(此处 M 是波点数)作为评价函数。表 2 为最优化前后的各层光学厚度，图 7 为最优化后的八层膜系计算的光谱特性曲线。在上述波长区，经最优化后，最大的一点为 $R_{max}=0.024$。可以看出，经随机调优后的八层膜显著地改善了初始八层膜系的光谱曲线。使之在 2～14 μm 光谱区能有比较高的增透性能，这充分显示了"随机优选法"对光学膜系最优化的功能。

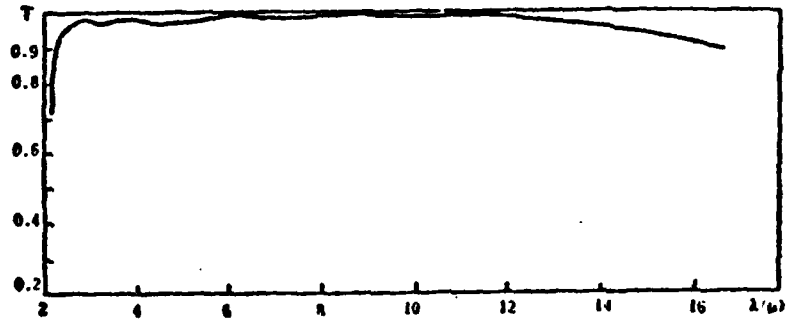

图 7　最优化后的八层计算光谱曲线($n_0=4$)

表 2　最优化前后八层厚度参数(单位: $\lambda_0/4$)

	X_1	X_2	X_3	X_4	X_5	X_6	X_7	X_8
优化前	1.24	0.48	0.24	1.36	0.24	0.58	0.54	0.22
优化后	1.2	0.19	0.265	1.347	0.114	0.536	0.348	0.219

前面计算的 $T\sim\lambda$ 曲线都是只考虑基片单面的增透效果，而基片的另一面是假定为无限延伸的，下面给出的实验结果是基片两面镀上同样的膜系的结果。

四、实验结果与分析

我们在普通光学多层设备(DMD-450)上用比较片倍波控制，并用非 $\lambda_0/4$ 控制曲线[4]，控制各层光学厚度。要镀出实用的宽带增透膜系是不太难的。重复实验时性能稍有变化，但每次实验曲线中透射率水平基本相同。图 8 是总层数为四层的等效三层宽带增透膜系之实验光谱特性曲线；图 9 乃是最优化后的八层超宽膜系光谱特性曲线。

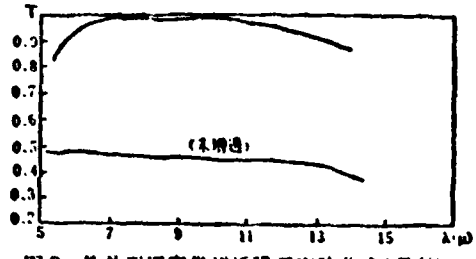

图 8　等效三层宽带增透膜系实验曲线(双面)

图 9 给出的实验曲线，虽具有较好的增透性能，但与计算值相比，偏离稍明显。这种偏离，一是因为在很宽的波长范围内，理论计算未考虑材料的色散和吸收，Ge、ZnS、SrF_2 在 18 μm 后都有一些吸收，在 8 μm 附近也存在水吸带的影响；二是普通光电极值膜控仪控制非 $\lambda_0/4$ 点误差较大，使实验曲线难以与计算值符合得很好。

尽管存在实验上的一些困难，然而对于 Ge 衬底的 8～14 μm 及 2～14 μm 范围的宽带增透曲线，平均透过率和最低一点的透过率都达到美国 OCLI 公司的商品指标。用于

8～14 μm 的宽带增透曲线在 8～12 μm 内平均透过率和最低一点透过率为 $\bar{T}_{8\sim12}$～97.5%，T_{min}～94.5%，用于 2～14 μm 的宽带增透曲线在 2.5～14 μm 内平均透过率和最低一点的透过率为 $\bar{T}_{2.5\sim14}$～94.6%，T_{min}～82.5%。

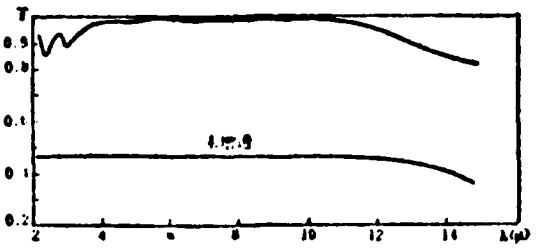

图 9　利用"随机最优化"法所获得的八层宽带增透膜系实验曲线(双面)

虽然在 2～14 μm 波长区能找到一些其他材料来满足宽带增透中某些层的需要，从而可能实现更好一些的光谱特性，但从实际应用上看，易溶解的、膜软的、毒性大的材料，对制作和使用都是不利的。因而作者选用了比较合适的材料 Ge、ZnS、SrF₂ 作为膜料，虽然在设计和制作上增加了一些困难，但还是较好地解决了 8～14 μm 及 2～14 μm 的宽带设计与制作课题。

本文的设计思想，原则上也适用于设计和制作其他高折射率衬底的宽带增透膜系。

致谢——作者向对本工作设计与制作给予帮助的陶凤翔、朱福荣等同志表示衷心感谢。

参 考 文 献

[1] L. Young, *J. Opt. Soc. Am.*, **51** (1961), 967.

[2] E. L. Church et al, *Appl. Opt.*, **13** (1974), 1274.

[3] H. A. Macleod, *Thin-Film Optical Filters*, London: Adam. Hilger. Ltd, 1969. 中译本：光学薄膜技术。周九林、尹树百译，国防工业出版社，1974.

[4] P. H. Berning, *J. Opt. Soc. Am.*, **52**(1962), 431.

[5] 陶凤翔，红外技术与技术，(1978), 4, 49.

[6] 张凤山，红外物理与技术，(1975), 3, 1.

DESIGN AND ANALYSIS OF INFRARED BROAD-BAND ANTIREFLECTION COATINGS

XU BUYUN

(Shanghai Institute of Technical Physics, Academia Sinica)

ABSTRACT

It has been done to optimize an infrared broad-band coating on the theory of equivalent multi-layers by means of a computer program named "Random optimization". The practical design and experimental results for 8～14 and 2～14 micrometer wavelength band on Ge substrate are presented.

END

FILMED

3-18-83

FTD

RAC

END

FILMED

2-85

DTIC